The application of fractional order control for an air-based contactless actuation system

Krijnen, Martijn; van Ostayen, Ron; Hossein Nia Kani, Hassan

DOI
10.1016/j.isatra.2017.04.014

Publication date
2017

Document Version
Accepted author manuscript

Published in
ISA Transactions

Link to formal publication "titel tijdschrift" (Elsevier): https://doi.org/10.1016/j.isatra.2017.04.014

The Application of Fractional Order Control for An Air-based Contactless Actuation System

Martijn E. Krijnen, Ron A. J. van Ostayen, Hassan HosseinNia

Department of Precision and Microsystem Engineering,
Delft University of Technology,
Delft, The Netherlands.

Abstract

Industry pushes towards ever faster and more accurate production of thin substrates. Contactless positioning offers advantages, especially in terms of risk of breakage and contamination. A system is considered designed for contactless positioning by floating a silicon wafer on a thin film of air. This paper focuses on the design of a control system, including actuators, sensors and control method, suitable for this purpose. Two cascaded control loops, with decoupled SISO controllers, are implemented for this moving mass controlled on a mass-spring system, which can be modelled as a fourth order system. The SISO controllers are first designed with classic loopshaping tools, which are then modified using fractional control. Two arguments based on examples in this system are given for the application of fractional control. Firstly, to increase the bandwidth of a regular mass-spring system, and secondly to control a plant which behaves fundamentally fractional, such as the moving mass in this cascaded fourth order system. By merely the application of fractionality, the bandwidths are extended by 14.6 % and 62 %, for the inner and outer loop respectively. A closed-loop positioning bandwidth of the wafer of 60 Hz is achieved, resulting in a positioning error of 104 nm (2 σ value), which is limited by sensor noise and pressure disturbances. This paper shows how the extension of classic loopshaping tools with fractional control can directly improve the performance, without adding to the complicatedness of the control system. Moreover it demonstrates a working concept of a novel type of contactless actuator.

Keywords: Fractional order control, Contactless actuation.

1. Introduction

Numerous production processes in high-tech industry are involved with thin and fragile sheets of material. During these steps the substrates are inspected, coated, exposed or patterns are printed on their surface, all of which are essential for their functionality. These substrates are often highly sensitive to contamination, impact or even breakage may occur at every mechanical contact. Handling these substrates without making contact could potentially solve these issues. On top of this, contactless handlers generally have a low moving mass which brings benefits regarding speed, and a negligibly small in-plane damping and stiffness.

At Delft University of Technology research has been done regarding a contactless handling system based on air-bearing technology, i.e. two surfaces with a thin film of pressurized air in between that separates both surfaces ([1], [2] and [3]). With this principle any type of substrate can be levitated and transported with low-friction. By applying a large vacuum preload on the substrate, the virtual mechanical out-of-plane stiffness of the substrate relative to the system can be increased substantially. As a result, any orientation of the system with respect to the field of gravity is possible, enabling contactless handling of the substrate in all orientations. In the experimental set-up under consideration the surface consists of an array of hexagonal surfaces, with a high pressure inlet in het middle, and a vacuum pressure along the sides. By tilting these surfaces, the air-flow beneath the substrate can be controlled, as illustrated in Figure 1. This array of tilting surfaces provokes

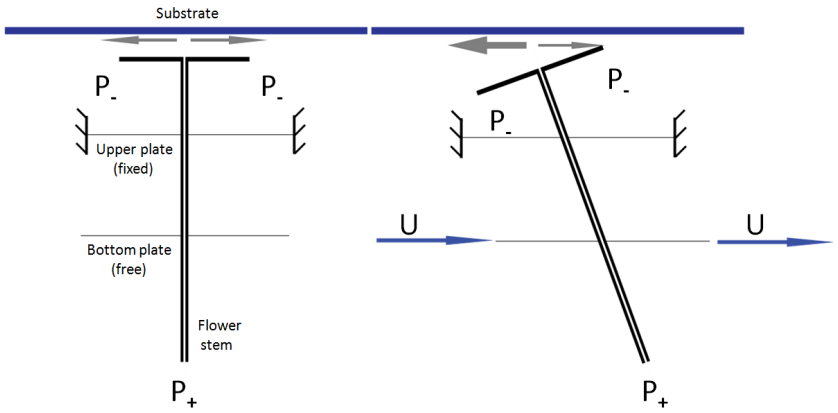

Figure 1: Basic principle of the air-bearing-based contactless actuator. A displacement input U provokes a flower angle, which induces a viscous force on the substrate.

images of fields of sunflowers, all tilting their heads in unison towards the sun. Therefore, the product was nicknamed the flowerbed. An image of the system is shown in Figure 2. The flower stem supplies the high pressure air to the surface, and is fixed in two membranes, one of which is fixed to the world, while the other can freely move, such that an angle can be imposed on the surface. In [2] the flowerbed technology was proven to work, but the system was not yet fully developed, only the system as shown in Figure 2. For a working positioning system, actuators, sensors and control need to be implemented.

Fractional-order control has been successfully developed during past two decades [4, 5, 6, 7, 8, 9, 10, 11, 12, 13, 14, 15, 16]. Tuning of fractional order PID controllers has also been extensively studied in [17, 18, 19, 20, 21, 22, 23, 24]. Despite these great efforts there still strong need for application such effective controllers to real practical application. In this paper, we bridge this gap and implement a fractional-order PID in a mechatronic application.

This paper describes the design and modelling of a feedback system for the flowerbed, and shows the contribution of fractional control. Actuators, sensing system and control are designed and implemented. Fractional control applied to reach the highest bandwidth possible, which could not be done using integer order control, based on two arguments. The first is that fractional control allows for extra design freedom, leading to a more perfectly suited controller. This extra parameter can lead us toward higher robust bandwidth that is not possible using integer order PIDs. The higher order lead control increase phase but decreases the robustness margin. Fractional order lead control will be trade off between higher bandwidth and stability. The second is to control a plant dynamics, which behaves fractional, such as the moving mass of a cascaded fourth order system It also describes the practical implementation and physical results of these methods, and gives the first demonstration of the working concept of a novel contactless actuation system.

In the next Section, elctromagnetic actuators are implemented and the entire system is modelled. Then in Section 3 the control system is designed, of which the results are given in Section 4. Finally a Discussion and Conclusion are given in Sections 5 and 6 regarding control and regarding the positioning system.

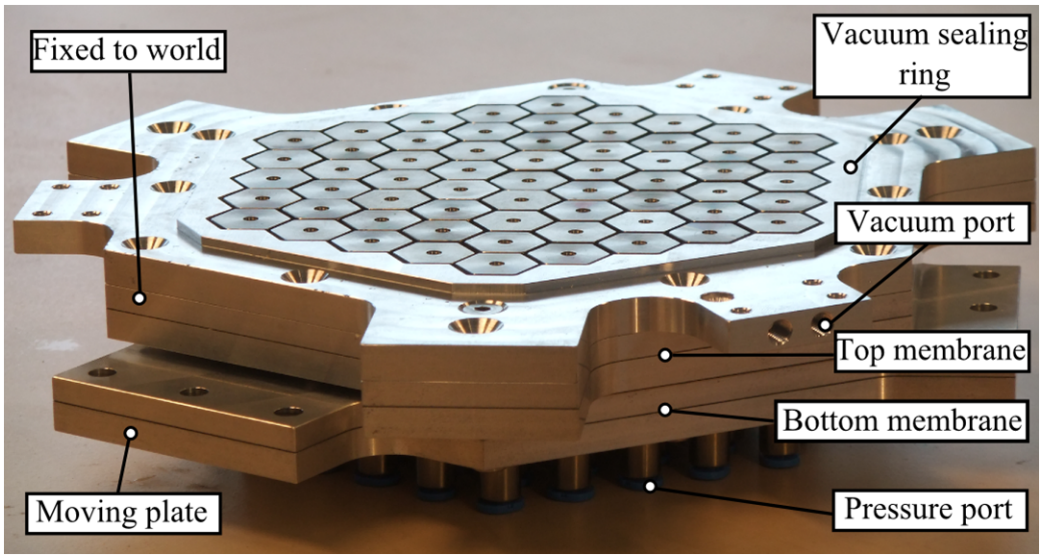

Figure 2: Overview of the flowerbed.

2. Modelling and Design of the Actuator

The Moving Plate in Figure 2 determines the angle of the surface by moving in-plane (as illustrated in Figure 1), therefore its position will be controlled in 3 degrees of freedom (two degree of freedom translations and a rotation). The actuators chosen to actuate the moving plate, are electromagnetic actuators, making use of the principle of variable reluctance. Per actuator, two coils are set opposing each other, with a ferromagnetic target in between, which is attached to the moving plate. The whole moving mass is shown in Figure 3. Its position is measured by three collocated capacitive sensors. The deformation of the membranes provides a stiffness to this moving mass. The actuators are linearized using an approximation of the measured relationship to compensate the inherent nonlinearity, as proposed by [25].

Now a simplified 1-D model can be proposed of the overall system and its subsystems (See Figure 4). These subsystems behave as follows: the actuators provide a force onto the mechanical system, which can be modelled as to a mass-spring system. The pneumatic transfer, from flower angle to force on the wafer, can be modelled by a proportional gain K_{pn} for the frequency-range of interest [2], and then the wafer can be seen as a moving

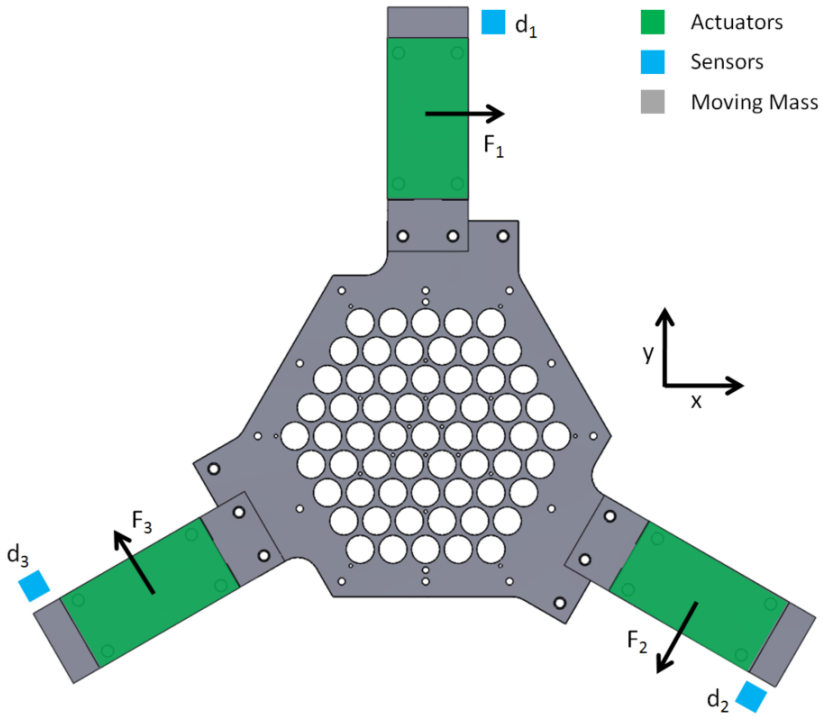

Figure 3: Moving mass which is actuated by the electromagnetic actuators.

mass, denoted by m_w.

$$\frac{x_w}{F} = \frac{K_{\text{pn}}}{m_{\text{w}} s^2 (ms^2 + k)} \tag{1}$$

This 1-D model shows a 180 degrees phase lag at 0 Hz, and a 360 degrees phase lag after its fundamental eigenfrequency $f_0 = \frac{1}{2\pi}\sqrt{\frac{k}{m}} = 39.6Hz$, thus limiting the theoretical bandwidth, of a single loop controller, to below this eigenfrequency. The proposed solution is Cascade Control, shown in Figure 4. The inner loop maintains an approximately 0 dB transfer up to its bandwidth frequency, and maintains the phase close to zero. In other words it reduces the order of the system as seen by the Outer Loop Controller (OLC) to approximately 0 up until its bandwidth. In this way the outer loop can be closed at a frequency higher than f_0.

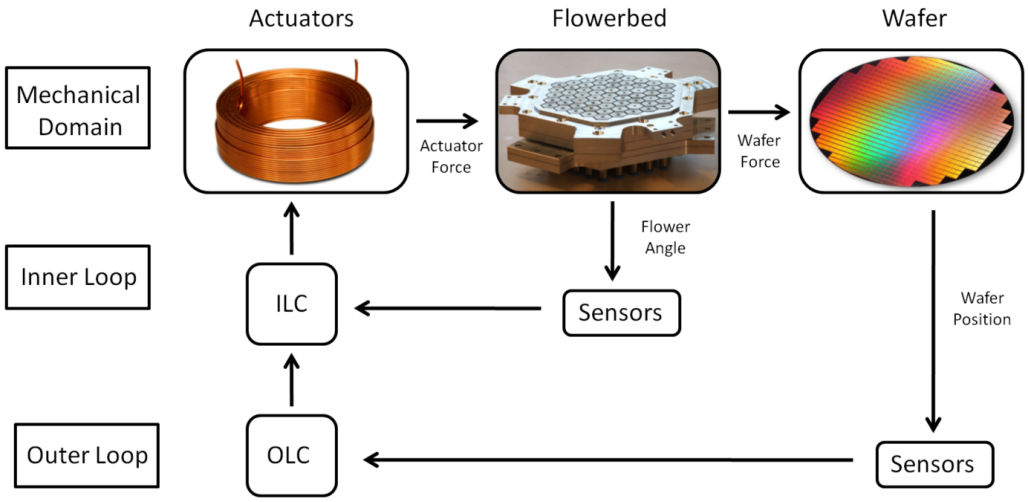

Figure 4: Proposed Control Strategy, with an Inner Loop Controller (ILC) and an Outer Loop Controller (OLC).

2.1. Modelling

The plant of the inner loop can be reduced to a mass-spring system, but can more accurately be modelled, by calculating the compliance from the actuator force vector $[F_1\ F_2\ F_3]$ to the sensor displacement $[d_1\ d_2\ d_3]$, denoted in Figure 3. This is done using finite element based frequency analysis, and results in a 3×3 transfer matrix. It is possible to decouple this plant into

global coordinates $[X\ Y\ \theta]$ with three corresponding transfer functions, using the following coordinate transformation matrices:

$$\begin{bmatrix} F_1 \\ F_2 \\ F_3 \end{bmatrix} = \begin{bmatrix} \cos\theta_1 & \sin\theta_1 & L_F \\ \cos\theta_2 & \sin\theta_2 & L_F \\ \cos\theta_3 & \sin\theta_3 & L_F \end{bmatrix} \begin{bmatrix} F_x \\ F_y \\ M_\theta \end{bmatrix} \tag{2}$$

$$\begin{bmatrix} u_x \\ u_y \\ u_\theta \end{bmatrix} = \begin{bmatrix} \cos\theta_1 & \cos\theta_2 & \cos\theta_3 \\ \sin\theta_1 & \sin\theta_2 & \sin\theta_3 \\ L_d & L_d & L_d \end{bmatrix} \begin{bmatrix} d_1 \\ d_2 \\ d_3 \end{bmatrix} \tag{3}$$

where L_F and L_d are the distances from center to the point of force application and sensor location, θ_1-θ_3 are the angles between actuators and global coordinate frame, and F_x-M_θ and u_x-u_θ are the forces and displacements in the global coordinate frame. The decoupling is demonstrated in Figure 5.

The frequency domain plant analysis results in a parametric model of the plant. Comparing this to an Empirical Transfer Function Estimation (ETFE) and minimizing the error results in a set of parametric transfer functions.

For clarity, troughout the rest of this paper only a single decoupled translational degree of freedom (DoF) is considered. In reality everything is designed and implemented in 3-DoF, of which the rotational is significantly different to the two translational DoF, but the same approach applies.

The ETFE and the reduced and fitted model is shown in Figure 6. Its transfer function is given by:

$$G(s) = e^{-\tau s} \cdot \sum_{1}^{N} \frac{1}{m_i s^2 + c_i s + k_i} \tag{4}$$

For a number of modes N which are defined by the modal masses m_i, modal damping c_i and k_i, whose values, along with the modal frequency, are given in the following table.

The badly damped eigenmodes of the electromagnetic actuators limit the achievable bandwidth. When using PID control, only the first mode after the bandwidth frequency (369 Hz), and the mode with the highest amplitude (1020 Hz) really limit the bandwidth. Therefore only these two higher modes are retained in the model.

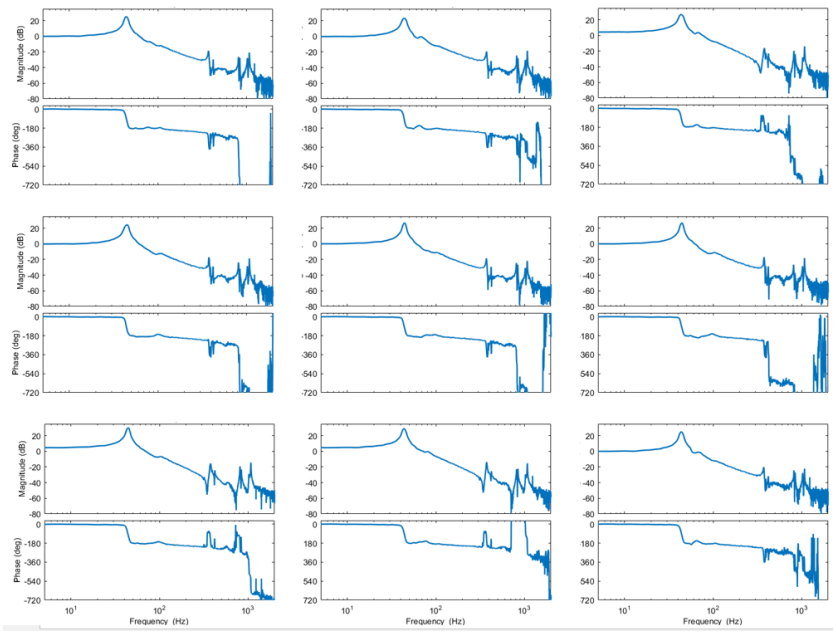

(a) Nominal plant, $[F_1, F_2, F_3]$ to $d_1, d_2, d_3]$

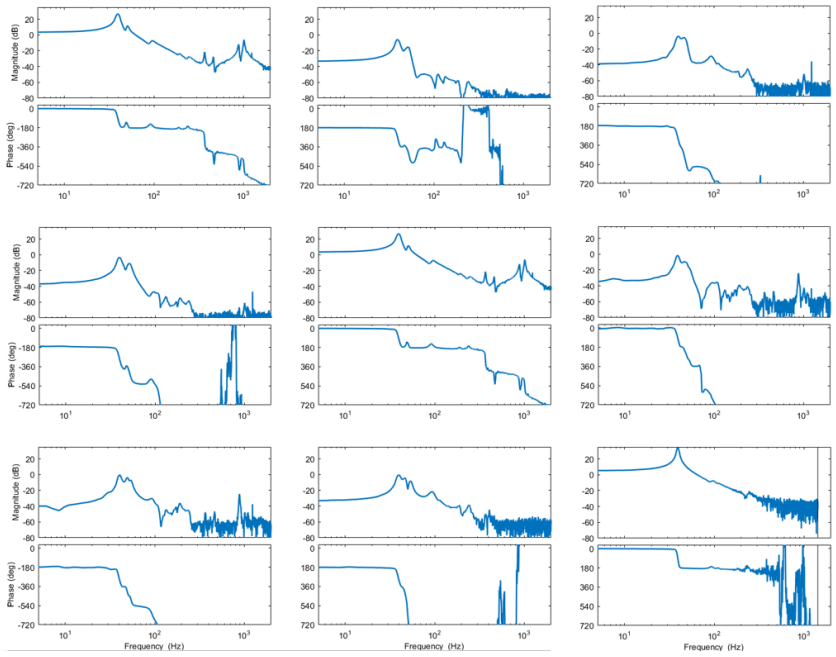

(b) Decoupled plant, $[F_x, F_y, F_\theta]$ to $u_x, u_y, u_\theta]$

Figure 5: Decoupling using the transformation matrices from equation 2 and 3

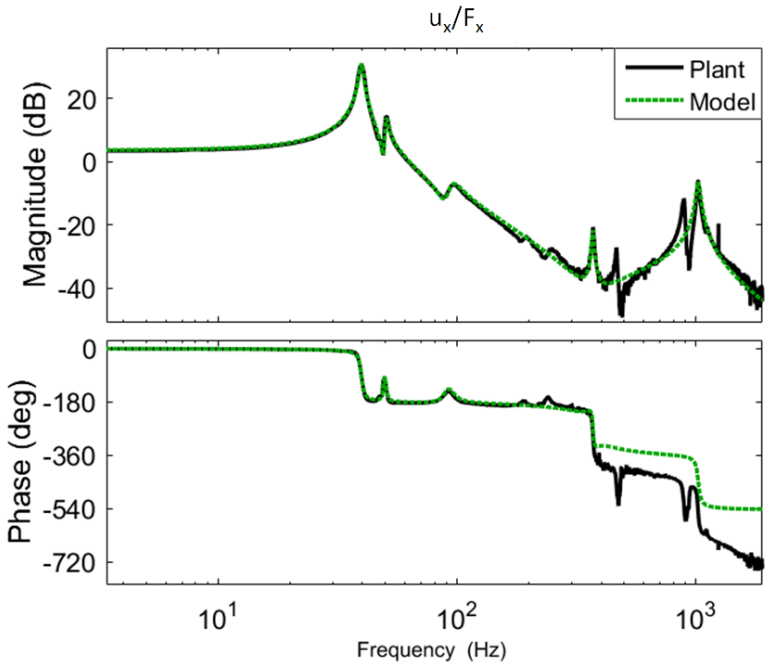

Figure 6: Parametrically identified model where only the two most limiting higher eigenmodes were retained in the model for control design.

Mode	m_i	c_i	k_i	f (Hz)
1	1.184×10^{-5}	1.120×10^{-4}	0.7332	39.6
2	1.261×10^{-4}	0.103	12.50	50.7
3	1.062×10^{-4}	8.00×10^{-3}	37.04	96.5
4	1.86×10^{-4}	5.348×10^{-6}	1005	369
5	2.029×10^{-6}	3.682×10^{-4}	83.33	1020

Table 1: Modal parameters for the parametrized model (Figure 1). A delay of $\tau = 0.0001s$ is added to the model.

3. Control Design

3.1. Fractional order Control

Fractional order derivatives are n-th order derivatives where n is not an integer. The motivation to use fractional-order PID is to improve the performance of the system like bandwidth that is not possible with the classical PID controllers. Many different ways to approximate fractional order derivatives are available, an overview is given in [26]. In this project the CRONE approximation is used, by far the most popular type, proposed by Oustaloup in 1991 [27].

Consider the ideal model of the flowerbed discussed in Section 2, a moving mass actuated by a mass spring system. All eigenmodes shown in Figure 6 except the fundamental (lowest frequency) mass-spring mode are omitted. For generalization the basic PID rules of thumb, proposed and extensively explained in [28], are applied, which are given by:

$$C_{\mathrm{PID}}(s) = K_p(1 + \frac{\omega_i}{s}) \cdot \frac{\frac{s}{\omega_z} + 1}{\frac{s}{\omega_p} + 1} \tag{5}$$

$$K_p = \frac{G(\omega_{bw})}{3}$$
$$\omega_z = \frac{\omega_{bw}}{3}$$
$$\omega_p = 3 \cdot \omega_{bw}$$
$$\omega_i = \frac{\omega_{bw}}{10}$$

where ω_{bw} is a given target bandwidth and G is a plant transfer function. This may be compared with a fractional version, using a real (non-integer) number q, constituting PID^q:

$$C_{\mathrm{PID},f}(s) = K_p(1 + \frac{\omega_i}{s}) \cdot \left(\frac{\frac{s}{\omega_z} + 1}{\frac{s}{\omega_p} + 1} \right)^q \tag{6}$$

Similar versions of fractional PID are discussed in [8] and [29], and applied in [30]. In Figure 7 a comparison is made for C_{PID} and $C_{\mathrm{PID},f}$ for $q = 1.1$. Regardless of the value of ω_{bw}, PID produces a phase lead of 47.91 degrees, PID$^{1.1}$ of 59.28 degrees (an increase factor of 1.24). The negative phase (delay) produced by a sampling time $t_s = 1 \cdot 10^{-4}$ is calculated for three frequencies of interest in Table 2. This example shows that, for a

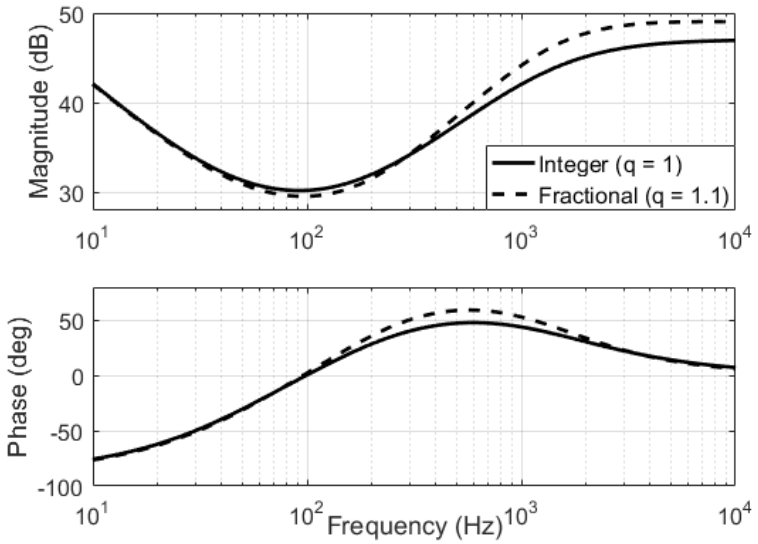

Figure 7: Comparison of PID and PID$^{1.1}$, using the PID rules of thumb (Equation 5)

Frequency (Hz)	100	500	800
Phase (deg)	-3.6	-18	-28.8

Table 2: Phase lag due to the inherent delay caused by a sampling time of $t_s = 0.1$ ms. PID adds 47.91 degrees and PID$^{1.1}$ adds 59.28 degrees.

Phase Margin of 30 degrees, the bandwidth of PID is limited by the delay to approximately 500 Hz. By applying PID$^{1.1}$ the bandwidth for the same phase margin is limited to approximately 800 Hz. This simple extension of PID thus increases the bandwidth with a factor 1.6.

Another motivation to use fractional order derivative in our application is to have a trade off between increasing the phase margin and increasing the gain at high frequencies. We are interested in increasing the phase margin since it increase the stability and therefore the bandwidth can increase. But we are not interested in increasing the gain at high frequency since it jeopardizes the modules margin (increases the peak of sensitivity function i.e. $\max_\omega \left|\frac{1}{1+L(\omega)}\right|$ and $L(\omega)$ is the open loop transfer function) and therefore reduces the robust bandwidth. Let us consider the following lead filter:

$$\left(\frac{\frac{s}{\omega_z}+1}{\frac{s}{\omega_p}+1}\right)^q, \tag{7}$$

where $\omega_z = \omega_{bw}/a$ and $\omega_p = a\omega_{bw}$ are the frequencies where the differentiation starts and stops and q is the order of differentiator. Considering a to be a scaling factor, the compensated phase at bandwidth frequency ω_{bw} is:

$$\phi_C = q(\tan^{-1}(a) - \tan^{-1}(\frac{1}{a})), \tag{8}$$

Where ω_{bw} is also crossover frequency if proportional gain in(6) is chosen as:

$$K_p \approx \frac{1}{a^q|G(\omega_{bw})|} \tag{9}$$

Figure 8 compares three different lead filters that compensate about 80-degree at ω_{bw}:

- Filter #1 (green line, $q = 1$), is a first order filter with long differentiation band i.e. $a = 10$.
- Filter #2 (purpule line, $q = 2$), is a second order filter with short differentiation band i.e. $a = 2.1$.
- Filter #3 (blue line, $q = 1.5$), is a fractional-order lead filter that uses a trade off between Filter #1 and Filter #2 i.e. $a = 3$.

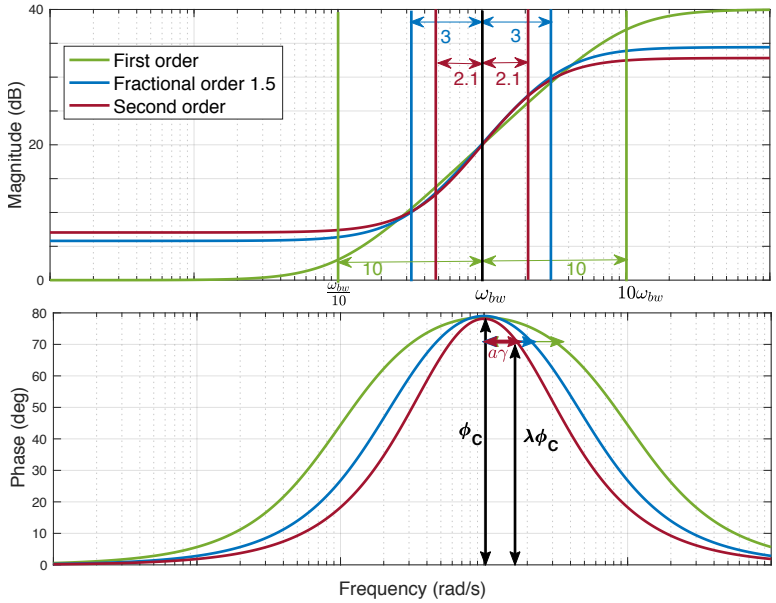

Figure 8: Comparing different lead filters to compensate about 80°

First order filter attenuates the high frequency modes less than second order and fractional order one (with the order greater than 1). It is very important factor to consider in practical system since high frequency modes (these modes in our system are located above 360Hz) limit the bandwidth and modulus margin. The Modulus Margin describes the shortest distance from the Nichols or Nyquist curve to the critical point, and is therefore defined as:

$$\mathrm{MM} = \|1 + L\|_{\min} \tag{10}$$

Where $L(\omega) = C_{\mathrm{PID},f}(\omega)G(\omega)$ is loop gain and $C_{\mathrm{PID},f}$ is the controller as defined in (6) and G is the system dynamics. In order to study the effect of high frequency modes in modulus margin, this controller is simplified at high frequency as:

$$\lim_{\omega\to\infty} C_{\mathrm{PID},f}(\omega) = K_p \left(\frac{\omega_p}{\omega_z}\right)^q = \frac{1}{a^q|G(\omega_{bw})|}\left(\frac{a\omega_{bw}}{\omega_{bw}/a}\right)^q = \frac{a^q}{|G(\omega_{bw})|} \tag{11}$$

Substituting (11) into (10) we have:

$$\mathrm{MM} = \|1 + L\|_{\min} = \|1 + a^q \frac{G(\omega)}{|G(\omega_{bw})|}\|_{\min} \tag{12}$$

Suppose $|G|$ and $\angle G$ are the absolute value and the phase of $G(\omega)$, respectively, (12) can be rewritten as:

$$\mathrm{MM} = \|1 + a^q \frac{G(\omega)}{|G(\omega_{bw})|}(\cos(\angle G) + j\sin(\angle G))\|_{\min} =$$

$$\min\sqrt{\left(1 + a^q \frac{G(\omega)}{|G(\omega_{bw})|}\cos(\angle G)\right)^2 + \left(a^q \frac{G(\omega)}{|G(\omega_{bw})|}\sin(\angle G))\right)^2} =$$

$$\min\sqrt{1 + a^q \frac{G(\omega)}{|G(\omega_{bw})|}\left(2\cos(\angle G) + a^q \frac{G(\omega)}{|G(\omega_{bw})|}\right)} \qquad (13)$$

Assuming $\left(2\cos(\angle G) + a^q \frac{|G(\omega)|}{|G(\omega_{bw})|}\right) < 0$, for the fractional order $1 \leq q \leq 2$ and $a \geq 1$ (it is a fair assumption since $a < 1$ results in an insignificant phase margin), it is obvious from (8) and (13) that increasing a and/or q will increase the phase margin which is desired while it decreases the modulus margin. If $\left(2\cos(\angle G) + a^q \frac{|G(\omega)|}{|G(\omega_{bw})|}\right) > 0$, decreasing q and a will decrease the modulus margin while it will decrease the phase margin, undesirably. In both cases, the fractional order lead control will be beneficial over first or second order lead filter.

In addition, for the same phase margin, second order filter has very narrow phase compensation compared to first order and fractional order one which makes the controller sensitive to the gain variation. In order to understand this better, let us define a robust band γ that guarantees phase of the controller to be above $\lambda\phi_C$ (γ and λ are graphically shown in Figure 8). Therefore, we have:

$$\lambda\phi_C = q(\tan^{-1}(a\gamma) - \tan^{-1}(\frac{\gamma}{a})) \qquad (14)$$

From (14) and Figure 8, one can conclude that for a given ϕ_c and $\lambda < 1$, increasing q decreases the robust band i.e. $a\gamma$. This is another important factor to be considered in practical system for the robustness against uncertainty in the model.

Therefore, fractional order lead filter is a conservative choice to obtain the higher robust bandwidth that is a trade off between higher phase margin, higher modulus margin and higher bandwidth. This is an argument for the application of fractional control, which will be applied in Section 4.1 in the inner loop. Here follows a second argument, based on the control of a fractional plant, as applied in the outer loop in Section 4.2.

Still using the ideal fourth-order model presented in Section 2, the transfer as seen by the OLC, controlling the moving mass, is shown in Figure 9. In this idealized model, the inner loop causes the moving mass to act 'un-ideal'. The slope of the outer loop is not exactly -2, but in fact closer to -1.3 around the cross-over frequency of the inner loop. When adding PID control, the lower steepness due to the controller's +1 slope, can lead to very thin stability margins. This can be improved by increasing the inner-loop phase margin, by lowering the cross-over frequency. Using the same rules of thumb in the previous section, a cross-over frequency of 100 Hz in the inner loop leads to a phase margin of 45 degrees (See Table 2), which almost halves the height of the closed-loop peak in the inner loop. But since the bandwidth of the inner loop is now 5 times lower, the outer loop bandwidth will also be approximately 5 times lower. In this paper, instead of classic integer order PID control, fractional control is proposed as a solution to deal with this specific case of a fractional plant (Section 4.2).

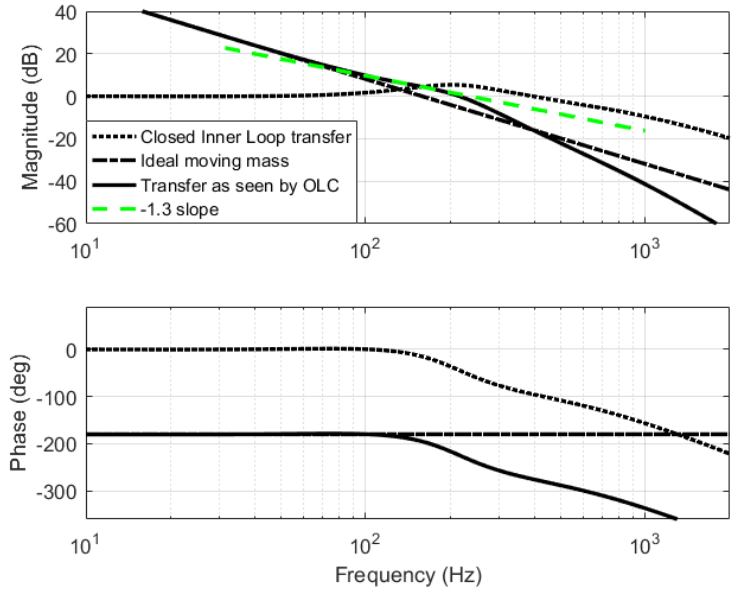

Figure 9: Demonstration of the effect of the inner loop on the outer loop transfer.

3.2. Loopshaping

A typical control approach for the decoupled 3-DoF cascaded control system, would be to implement a SISO PID-controller for each degree of

freedom, for both the inner- and outer loop.

A Proportional-Integrator (PI) block is implemented to achieve a proper gain, especially at low freqeuncies. The lead compensator (LC) is used to ensure stability. It adds phase around the targeted cross-over frequency, to ensure a proper Phase Margin (PM). However, the LC also increases the gain at higher frequencies. To reduce this effect and to deal with the higher eigenmodes a Low-Pass filter (LP) is implemented. These separate blocks are defined as:

$$PI(s) = K_p(1 + \frac{\omega_i}{s}) \tag{15}$$

$$LC(s) = \frac{\frac{s}{\omega_z} + 1}{\frac{s}{\omega_p} + 1} \tag{16}$$

with $\omega_z < \omega_c < \omega_p$.

$$LP(s)|_{n=3} = \frac{1}{\frac{s^2}{\omega_{lp}^2} + \frac{s}{\omega_{lp}} + 1} \frac{1}{\frac{s}{\omega_{lp}} + 1} \tag{17}$$

The low-pass filter LP is a butterworth filter of order $n = 3$, which can be chosen differently as preferred. The SISO controller transfer function is given as the series combination of these three functional blocks.

$$C(s) = K_p(1 + \frac{\omega_i}{s}) \left(\frac{\frac{s}{\omega_z} + 1}{\frac{s}{\omega_p} + 1} \right) \left(\frac{1}{\frac{s^2}{\omega_{lp}^2} + \frac{s}{\omega_{lp}} + 1} \frac{1}{\frac{s}{\omega_{lp}} + 1} \right) \tag{18}$$

By making the LC and LP fractional, using real number coefficients q and r, the slopes can be taken into account in the design, increasing the design freedom:

$$LC_f(s) = \left(\frac{\frac{s}{\omega_z} + 1}{\frac{s}{\omega_p} + 1} \right)^q, \tag{19}$$

$$LP_f(s)|_{n=3} = \frac{1}{\frac{s^{2r}}{\omega_{lp}^{2r}} + \frac{s^r}{\omega_{lp}^r} + 1} \frac{1}{\frac{s}{\omega_{lp}} + 1} \tag{20}$$

In [31] an extensive discussion of fractional butterworth filters is given, however for simplicity here an integer order butterworth filter is modified with a fractional order. [32] discusses a number of general fractional PID control design techniques.

In the next section, the controller parameter will be tuned through an optimization approach. However, more detail on tuning of the fractional order control can be found in literature [17, 18, 19, 24, 22, 6, 20, 23, 21].

3.3. Tuning

The set of parameters which can be used to tune these controllers is $x = [K_p, \omega_i, \omega_z, \omega_p, \omega_{lp}, n]$. In the fractional application this set of parameters is extended to $x_f = [K_p, \omega_i, \omega_z, \omega_p, \omega_{lp}, n, q, r]$.

An overview of rules to optimally tune a fractional PID controller, by optimization in the time-domain is given in [21], however in this paper a tuning optimization of the custom controller is performed in the frequency domain for the inner loop controller, maximizing the bandwidth. Stability margins were added as constraints, and then the optimization was executed using Matlab's optimization toolbox.

$$\begin{gathered} \min f(\omega_c) = \frac{\omega_{c,\mathrm{bm}}}{\omega_c(x)} \\ \text{s.t.} \\ \mathrm{PM} > 30 \text{ degrees} \\ \mathrm{GM} > 6 \text{ dB} \\ L(\omega_c) = 0 \end{gathered} \tag{21}$$

Where L is the loop-gain, and $\omega_{c,\mathrm{bm}}$ is the targeted bandwidth. A similar type of 'bandwidth-parameterization and optimization' was discussed by Gao in [20], as a general way to avoid an iterative tuning process. The optimization is based on the control transer functions as given in Equation 15 to 20 and the reduced model of the plant as given in Table 1. The results are given in Section 4.1.

3.4. Positive Position Feedback

Positive Position Feedback (PPF), a form of active damping, was implemented in the inner loop. This consists of a low-pass filter in a positive feedback loop, as shown in Figure 10. Around the corner-frequency of the low-pass filter PPF adds active damping, while in the low-frequency region it adds active flexibility (the open-loop gain is increased), while in the higher region it adds active stiffness. A similar application of PPF can be found in [33]. The transfer function is:

$$C_{\text{ppf}}(s) = \frac{g}{\frac{s^2}{\omega_f^2} + 2\epsilon\frac{s}{\omega_f} + 1} \tag{22}$$

where the parameters g, ω_f and ϵ are tuned by an optimization minimizing the difference between the closed plant and a butterworth filter. Here ω_f is a factor k_f higher than the eigenfrequency which is to be damped, which is in this case the fundamental eigenmode ω_0: $\omega_f = k_f\omega_0$

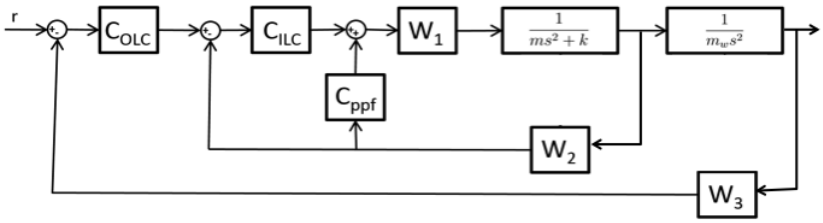

Figure 10: Control Structure including Positive Position Feedback (PPF)

3.5. MIMO and stability Analysis

After describing the control design in the SISO setting, an analysis of the behaviour of these components in the full MIMO setting is required. The overall open-loop MIMO transfer matrixes, for the inner loop L_{I} and outer loop L_{O} respectively, become:

$$L_{\text{I}} = C_{\text{ILC}}(C_{\text{ppf}}W_2PW_1)(1 - C_{\text{ppf}}W_2PW_1)^{-1} \tag{23}$$

$$L_{\text{O}} = \frac{C_{\text{OLC}}T_{\text{I}}}{m_w s^2} \tag{24}$$

Where T_{I} is the transmissibility function of the inner loop, and $m_w = 0.058$ kg is the wafermass. This MIMO analysis can be used to determine the Modulus Margin MM.

In the context of MIMO systems the Modulus Margin can be used as replacement of the GM.

Table 3: Calculated parameters for the PPF filter, using the model to be damped.

Parameters	Calculated value
g	0.5048
ϵ	0.5684
k_f	1.2123

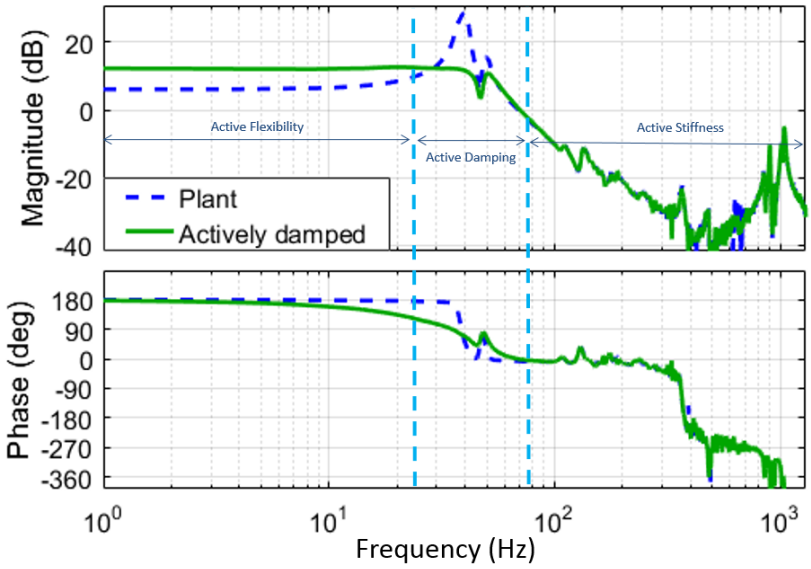

Figure 11: Effect of Positive Position Feedback

4. Results

4.1. Results Inner Loop

The calculated parameters for the Positive Position Feedback filter are shown in Table 3, and the effect on the transfer is shown in Figure 11.

The results of the SISO controllers are summarized for the case of the manual loopshaping, the optimization, and the optimization including fractional control in Table 4. The optimization was allowed to use any order of Low-Pass filter from 1 to 5, to determine which order gave the best performance. In both the integer controller and fractional controller, the 3rd order LP gave the highest bandwidth. The phase margin was maintained at exactly 30 degrees, and gain margins at exactly 6 dB. It is interesting to notice, that

the PID-benchmark controller is limited by Mode 4 (369 Hz), the optimized integer controller is limited by Mode 5 (1020 Hz), and the optimized fractional controller by both. This can be seen in the controller transfer function in Figure 12, where the integer and fractional controller coincide at the first limiting resonance, and the Fractional and Manual controller coincide at the second limiting resonance.

	Manual (IL)	Integer (IL)	Fractional (IL)	Manual (OL)
$f_{bw} = \omega_{bw}/2\pi$	101.8	107.9	122.5	60
K_P	0.854	0.497	0.406	9.6×10^5
$f_i = \omega_i/2\pi$	10	13.1	14.1	1
$f_z = \omega_z/2\pi$	30	15.7	14.2	6
$f_p = \omega_p/2\pi$	300	345.5	240.5	600
$f_{lp} = \omega_{lp}/2\pi$	400	396.3	412.2	400
q	1	1	1.2	0.9
r	1 (n=2)	1 (n=3)	0.81 (n=3)	1 (n=1)

Table 4: Tuning parameters for both the Inner Loop (IL) and Outer Loop (OL)

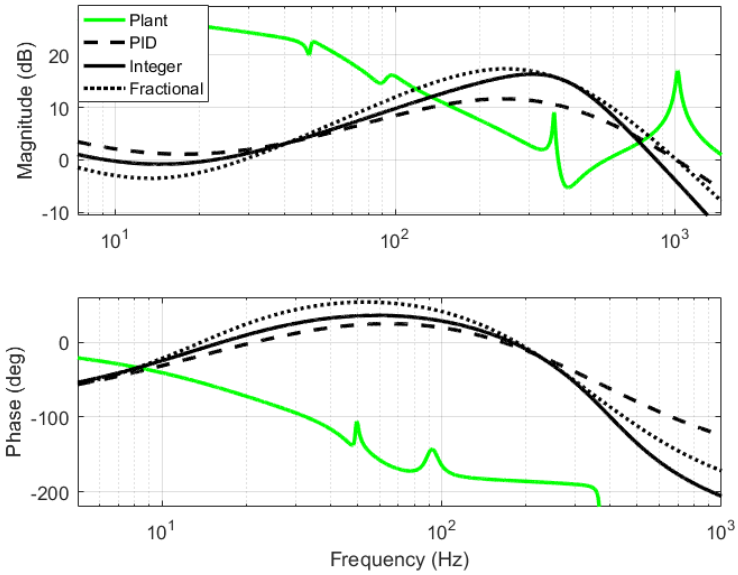

Figure 12: Comparison of inner loop controllers

The used CRONE approximations of the fractional transfer functions $LC_f(s)$ and $LP_f(s)$, based on the parameters in Table 4 are given below.

It was decided to keep the order of the approximation as small as possible without losing significant accuracy, which was achievable with third order approximations.

$$LC_f(s)|_{q=1.2} = \frac{24.29s^3 + 3760s^2 + 2.818 \times 10^5 s + 1.418 \times 10^6}{s^3 + 1495s^2 + 2.76 \times 10^5 s + 1.418 \times 10^6} \tag{25}$$

For the fractional low-pass filter, s^{1-r} was approximated, which was then implemented as in Figure 13, constituting the fractional part of the transfer function in Equation 20. This method reduces the order of derivative which has to be calculated each step, and there by reduces the required sampling time.

$$s^{1-r}|_{r=0.81} = \frac{1.928s^3 + 2008s^2 + 4.41 \times 10^4 s + 2.042 \times 10^4}{0.335s^3 + 723.5s^2 + 3.294 \times 10^4 s + 3.162 \times 10^4} \tag{26}$$

These equations approximate the transfer functions as determined by the

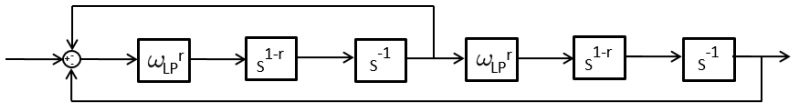

Figure 13: Implementation of the fractional low-pass filter.

parameters in Table 4, on the interval of 0.1 to 10000 Hz. The fractional controller and its approximation (without PI) is shown in Figure 14. The approximation increases the phase margin by 0.9 degrees and reduces the gain margin at 0.44 dB (at 369 Hz) because it has slightly higher gain in that regime. The high frequency gain is strongly reduced by this approximation, which is clearly favorable as it reduces the higher peaks and noise. This controller was implemented and resulted in a stable positioning system. In Figure 18a the closed-loop bode plot is shown.

The modulus margin calculated from the complete 3×3 transfer matrix does not differ from the 'ideally decoupled' transfer matrix (with zeroes on all non-diagonal entries). This is because after the decoupling, all non-diagonal entries remain below 0 dB (As shown in Figure 5), thereby not significantly affecting the controlled DoFs on the diagonal. The constraint on the Phase Margin can be seen in the Nyquist plots in Figure 15, as the two loop gains overlap when they cross the circle around the origin of magnitude 1, both

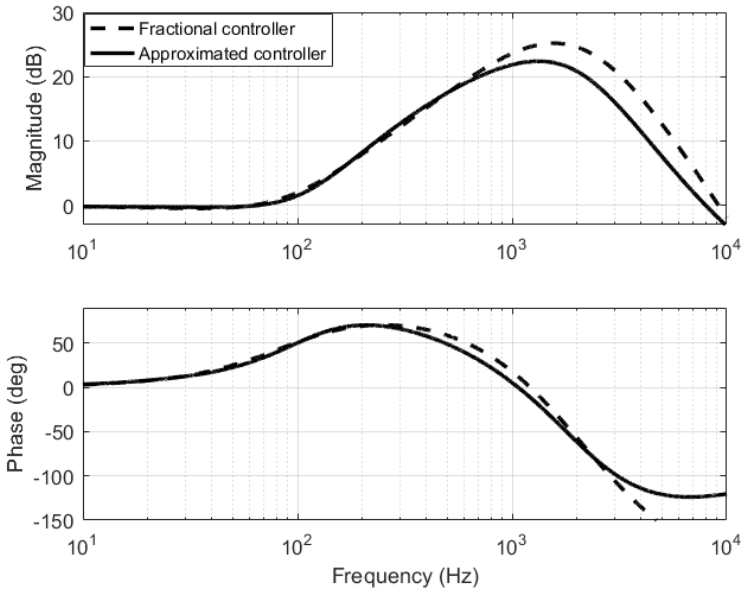

Figure 14: Approximation of the fractional controller

with a Phase Margin of 30 degrees. The constraint on the gain margin limits the magnitude of the higher eigenmodes to below 6 dB. However because the phase is not -180 (or -520) at these points, the gain margin found in Nyquist will be the gain where the phase crosses -180 for the first time, resulting in a margin of 6.57 dB for the integer controller and 6.1 dB for the Fractional Controller.

4.2. Results Outer Loop

The outer loop controller was tuned by manually iterative loopshaping. In Figure 16 the open-loop behavior 'as seen' by the OLC is shown in series with integer and fractional controllers . The controllers are shaped like the transfer function in Equation 18, with control parameters shown in the last column of Table 4. The Lead Compensator increases the gain around the targeted cross-over frequency, with a +1 slope, resulting in a gain margin of 1.6 dB. Because the Fractional Lead Compensator of order 0.9 has a lower positive slope, it retains a gain margin of 3.2 dB. For comparison, the bandwidth for which the integer PID controller would reach a gain margin of 3 dB is 37 Hz. For a Lead Compensator of order 0.8 the more negative phase reduces its performance. This tuning was done in the Nyquist domain, shown in Figure

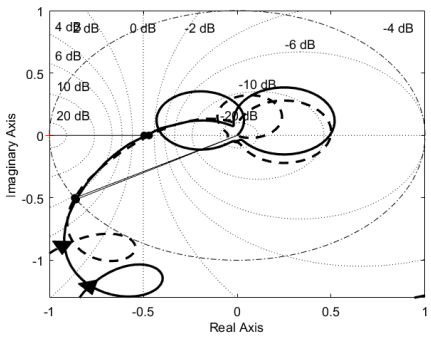

(a) Comparison of the Nyquist shapes of the Inner-Loop, using integer and fractional-order controller. The integer order has a slightly larger gain margin, but a significantly lower (14.6%) cross-over frequency.

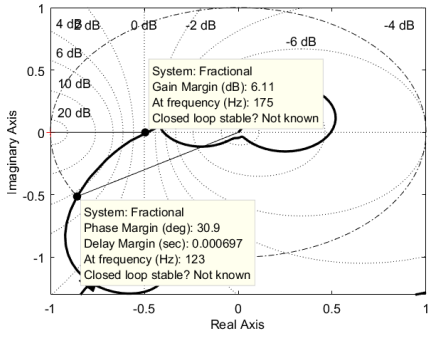

(b) Indicated Stability Margins in the Nyquist plot of the Open Inner-Loop with the Fractional Order Controller.

Figure 15: Nyquist stability analysis of the inner loop.

17. The best trade-off between high phase and steeper slope (higher gain margin) results from an analysis of modulus margin. When $q = 0.9$ modulus margin increases from 0.19 to 0.26, with respect to the integer controller, and the gain margin increases from 1.6 to 3.2 dB with a Phase margin of 40.2 degrees. Fractional order parameter $q = 0.8$ gives a bigger clockwise rotation of the Nyquist plot, thereby limiting the modulus margin to 0.18.

4.3. Results positioning system

Besides the control bandwidth, two main criteria are used to measure the performance of the motion system, being its precision and acceleration.

A minimum positioning error of 104 nm (2σ value) has been measured (Plot shown in Figure 19). This error is limited by internal sensor noise and unknown noise in the pressure lines, possibly due to turbulent flow.

The maximum achievable force was measured at 70 mN, resulting in a maximum acceleration of a 58 g wafer of 1.2 m/s^2. In measurement the maximum controlled acceleration which was achieved was 1.17 m/s^2. Higher accelerations were measured but there might have been contact between surface and wafer.

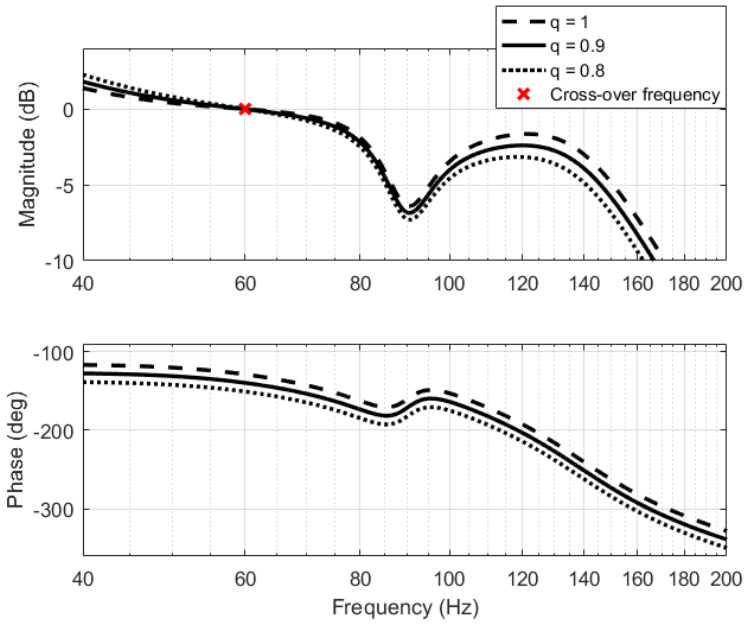

Figure 16: Comparison of open-loop transfers, using Fractional and integer controller in the outer loop. Both have their cross-over frequency at 60 Hz.

The inner loop produces a force on the wafer, and thereby imposes an acceleration. In reality the ILC can track any signal up until its bandwidth frequency, thereby limiting the derivative of acceleration (jerk) of the wafer.

$$\text{jerk}_{\max} = \frac{F_{\max}}{m_w} \cdot f_{\text{bw}} \tag{27}$$

A jerk-limiting motion profile as proposed by [34] was applied, which reduces high frequency content in the positioning error. In Figure 20 a plot is shown of the position, error and acceleration using the jerk-limited motion profile. The error remains within 2.1 μm during a 50 μm step. For comparison the error of a 50 μm instantaneous step-function is given in Figure 20b.

5. Discussion

The optimization of a pre-defined controller discussed in this paper, allows for better performance (compared to the PID rules of thumb) without losing control over the shape and complexity of the controller (as may be experienced in H_2/H_∞ optimal control). This keeps the control design relatively

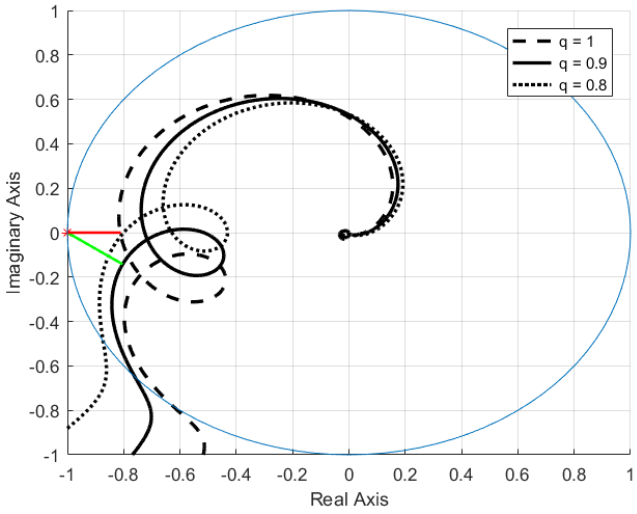

Figure 17: Nyquist of the Outer Loop, with shortest distance to -1 indicated in red for the integer controller, and in green for the fractional controllers. Using $q = 0.9$ increases the Modulus Margin from 0.19 to 0.26 and the Gain Margin from 1.6 dB to 3.2 dB (with a Phase Margin of 40.2 degrees). For $q = 0.8$ the more negative phase (clockwise rotation) reduces its performance.

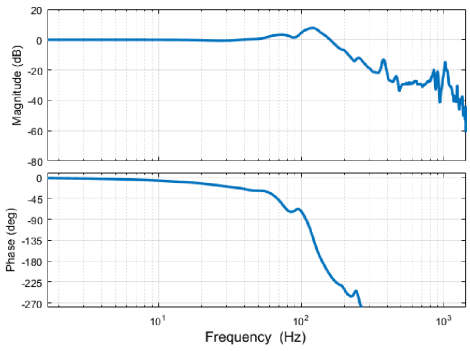

(a) Inner Loop, $f_{bw} = 122.5$ Hz

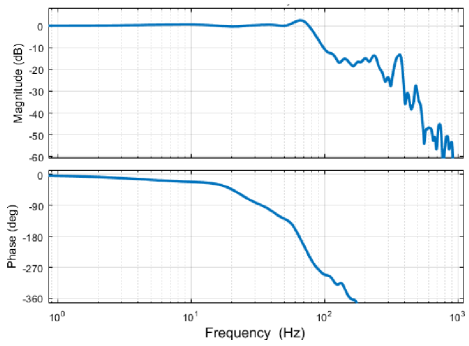

(b) Outer Loop, $f_{bw} = 60$ Hz

Figure 18: Closed Loop Transfer Functions of the implementation of the fractional controllers in the flowerbed.

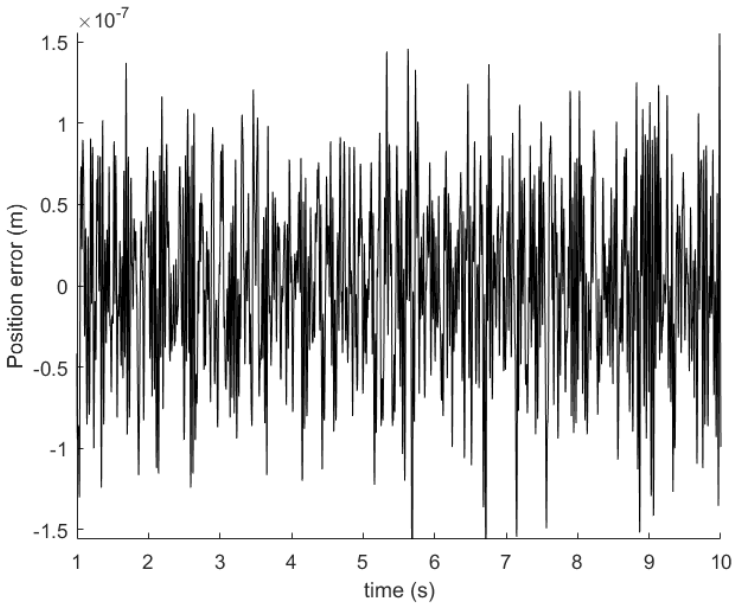

Figure 19: Plot of the positioning error

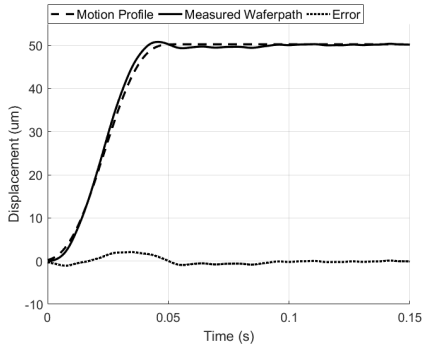

(a) Demonstration of the motion profile, performing a 50 μm step in 0.057 s. The error remains within 2.1 μm

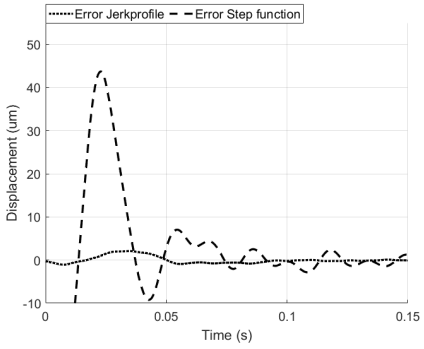

(b) Comparison of the error due to the motion profile and due to an instantaneous 50 μm step function.

Figure 20: Time response

simple and straight-forward. Nevertheless an H_2/H_∞ approach, optimizing all the control parameters, might improve performance. Also the Low-Pass filters are a simplification which can be omitted, by using truly fractional butterworth filters instead.

It has been discussed that the final controller for the outer-loop was found by manually iterative loop-shaping, using Bode and Nyquist analysis. A more optimal approach might be possible, however in case of the outer loop the uncertainty of the plant as seen by the OLC was much larger, due to pressure disturbances, and a not truly time-invariant system. This is due to the wire springs holding the wafer in range until it is in control, which have a different pretension every time they are attached and aligned. Therefore in the OLC the controller was manually shaped.

A generalization of the results regarding the OLC can be made, for most cascaded control systems. Whereas mechatronic engineers are mostly used to 0,-1 and -2 slopes, here the inner loop tends to affect the outer loop in a way which shows fractional slope behavior at the frequency range of interest.

The final bandwidth of the system would have been higher without the limiting eigenmodes in the inner loop, which are due to the masses of the reluctance actuators. A next version of this system would therefore demand an improvement in this area, e.g. by applying piezo actuators or a version of the reluctance actuators with higher and better damped eigenmodes.

6. Conclusion

The main contributions of this paper are the demonstration of a working concept of a novel contactless positioning system, and in the practical application of fractional control, which improves the system's performance in two different contexts.

A controller optimization where the design parameters of a predefined controller were optimized was applied. Including fractional control allowed for two extra design parameters, which increased the bandwidth by an additional 14.6%, while leaving the stability margins intact.

The measured transfer function in the outer loop of the fourth order system is a locally fractional transfer function, of an order of significantly less than 2, depending on the Phase Margin. Due to this, a lead compensator with a +0.9 slope can reach a significantly higher bandwidth than a lead compensator with a +1 slope (+62% when a gain margin of 3 dB is demanded). Using fractional control, a 122 Hz bandwidth was achieved for the inner loop,

controlling the flower position, and thereby the force on the wafer, while a 60 Hz bandwidth was achieved for the wafer position.

The highest attainable acceleration is determined by the waferforce and the wafermass. The maximum acceleration was measured at 1.17 m/s^2. The system can position the wafer with an accuracy of 104 nm (2σ).

References

[1] Jasper Wesselingh. *Contactless Positioning Using an Active Air-film.* PhD thesis, Delft University of Technology, 2011.

[2] Phuc Vuong. *Air-based contactless actuation system for thin substrates.* PhD thesis, Delft University of Technology, 2016.

[3] J van Rij, J Wesselingh, R A J van Ostayen, J W Spronck, R H Munnig Schmidt, and J van Eijk. Planar flat product transport using viscous traction. *International Joint Tribology Conference*, 2008.

[4] I. Podlubny. Fractional-order systems and $PI^{\lambda}D^{\mu}$ controllers. *IEEE Transactions on Automatic Control*, 44(1):208–214, 1999.

[5] Blas M. Vinagre, I. Podlubny, L. Dorcak, and V. Feliu. On fractional PID controllers: A frequency domain approach. In *Proceedings of the 2000 IFAC Workshop on Digital Control*, 2000.

[6] YangQuan Chen, Kevin L Moore, Blas M Vinagre, and Igor Podlubny. Robust PID controller autotuning with a phase shaper. In *Proceedings of the First IFAC Workshop on Fractional Differentiation and its Applications (FDA04)*, 2004.

[7] Blas M. Vinagre, C. A. Monje, A. J. Calderón, and J. I. Suárez. Fractional PID controllers for industry application. *Journal of Vibration and Control*, 13(9-10):1419–1429, 2007.

[8] H. Delavari, R. Ghaderi, A. Ranjbar, S. HosseinNia, and S. Momani. Adaptive fractional PID controller for robot manipulator. In *Proceedings of the 4th IFAC Workshop on Fractional Differentiation and Its Applications (FDA'10)*, 2010.

[9] J. Villagrá, V. Milanés, J. Pérez, and T. de Pedro. Control basado en pid inteligentes: Aplicación al control de crucero de un vehículo a bajas velocidades. *Revista Iberoamericana de Automática e Informática Industrial*, 7(4):44–52, 2010.

[10] Ching-Hung Lee and Fu-Kai Chang. Fractional-order PID controller optimization via improved electromagnetism-like algorithm. *Expert Systems with Applications*, 37:8871–8878, 2010.

[11] Celaleddin Yeroglu and Nusret Tan. Classical controller design techniques for fractional order case. *ISA Transactions*, 50(3):461 – 472, 2011.

[12] S. H. HosseinNia, I. Tejado, B. M. Vinagre, V. Milanés, and J. Villagrá. Low speed control of an autonomous vehicle using a hybrid fractional order controller. In *Proceedings of the 2nd international conference on control instrumentation and automation (ICCIA'11)*, 2011.

[13] Blas M. Vinagre and Concepción A. Monje. Fractional-order PID. In Ramon Vilanova and Antonio Visioli, editors, *PID Control in the Third Millennium*, pages 465–493. Springer London, 2012.

[14] S H HosseinNia, I Tejado, and B M Vinagre. Robust fractional order PI controller for switching systems. *Fifth Symposium on Fractional Differentiation and its Applications*, 2012.

[15] Inés Tejado, S. H. HosseinNia, Blas M. Vinagre, and Yang Quan Chen. Efficient control of a SmartWheel via internet with compensation of variable delays. *Mechatronics*, 23:821–827, 2013.

[16] S Hassan Hosseinnia, Inés Tejado, Vicente Milanés, Jorge Villagrá, and Blas M Vinagre. Experimental application of hybrid fractional-order adaptive cruise control at low speed. *IEEE Transactions on Control Systems Technology*, 22(6):2329–2336, 2014.

[17] R. Caponetto, L. Fortuna, and D. Porto. A new tuning strategy for a non integer PID controller. In *Proceedings of the 1st IFAC Workshop on Fractional Differentiation and its Applications (FDA'04)*, 2004.

[18] Duarte Valério and José Sá da Costa. A review of tuning methods for fractional PIDs. In *Proceedings of the 4th IFAC Workshop on Fractional Differentiation and Its Applications (FDA'10)*, 2010.

[19] Y. Luo and Y. Q. Chen. Fractional order [proportional derivative] controller for a class of fractional order systems. *Automatica*, 45(10):2446–2450, 2009.

[20] Z Gao. Scaling and bandwidth parameterization based control tuning. In *American control conference*, 2006.

[21] Fabrizio Padula and Antonio Visioli. Tuning rules for optimal PID and fractional-order PID controllers. *Journal of Process Control*, 21(1):69–81, 2011.

[22] Saptarshi Das, Suman Saha, Shantanu Das, and Amitava Gupta. On the selection of tuning methodology of FOPID controllers for the control of higher order processes. *ISA Transactions*, 50(3):376 – 388, 2011.

[23] Duarte Valério and José Sá da Costa. Tuning of fractional PID controllers with Ziegler-Nichols-type rules. *Signal Processing*, 86(10):2771–2784, 2006. ISSN 0165-1684.

[24] Indranil Pan, Saptarshi Das, and Amitava Gupta. Handling packet dropouts and random delays for unstable delayed processes in NCS by optimal tuning of controllers with evolutionary algorithms. *ISA Transactions*, 50(4):557 – 572, 2011.

[25] Yu-Ping Liu, Kang-Zhi Liu, and Xiaofeng Yang. Nonlinear current control for reluctance actuator with hysteresis compensation. *Journal of Control Science and Engineering*, October 2014.

[26] B.M. Vinagre, I. Podlubny, A. Hernandez, and V. Feliu. Some approximations of fractional order operators used in control theory and applications. *Fractional calculus and applied analysis*, 3(3):231–248, 2000.

[27] A Oustaloup. La commande crone: commande robuste d'ordre non entier. *Paris: Hermès*, 1991.

[28] R. Munnig-Schmidt, G. Schitter, A. Rankers, and J. van Eijk. *The Design of High Performance Mechatronics*. IOS Press, 2014.

[29] S Das, I Pan, and S Das. Performance comparison of optimal fractional order hybrid fuzzy PID contcontrol for handling oscillatory fractional order processes with dead time. *ISA transactions*, 52(4):550–566, 2013.

[30] I Tejado, V Milanes, J Villagra, J Godoy, H HosseinNia, and B M Vinagre. Low speed control of an autonomous vehicle by using a fractional PI controller. In *Proceeding: 18th IFAC World Congress*, 2011.

[31] A Acharya, S Das, I Pan, and S Das. Extending the concept of analog butterworth filter for fractional order systems. *Signal Processing*, 94: 409–420, 2014.

[32] C Yeroglu and N Tan. Classical control design techniques for fractional order case. *ISA Transactions*, 50(3):461–472, 2011.

[33] I A Mahmood and S R Moheimani. Making a commercial atomic force microscope more accurate and faster using positive position feedback control. *Review of Scientific Instruments*, 80.6, 2009.

[34] ML Norg M Steinbuch. Advanced motion control: An industrial perspective. *European Journal of Control*, 4(4):278–293, 1998.